Applied Acoustics 155 (2019) 180–189

Contents lists available at ScienceDirect

Applied Acoustics

journal homepage: www.elsevier.com/locate/apacoust

Monitoring the internal quality of ornamental stone using impact-echo testing

V. Montiel-Zafra [a,*], F. Canadas-Quesada [a], M.J. Campos-Suñol [b], P. Vera-Candeas [a], N. Ruiz-Reyes [a]

[a] Telecommunication Engineering Department, Linares School of Engineering, University of Jaén, 23700 Linares, Spain
[b] Geology Department, Linares School of Engineering, University of Jaén, 23700 Linares, Spain

ARTICLE INFO

Article history:
Received 17 October 2018
Received in revised form 16 May 2019
Accepted 27 May 2019

Keywords:
Non-destructive testing
Impact-echo
Ornamental stone
NLS
P-wave velocity
Intact
Damage

ABSTRACT

The decay and durability of stone materials is a natural response to the progressive adjustment to different environmental and harsh conditions. Usually stone building elements with no apparent sign of decay are affected by the loss of cohesion. Non-invasive, early and low-cost identification of the internal damage of stone materials would be a great step forward.

This paper presents an impact-echo (IE) method to analyse the internal quality of ornamental stone. The proposed method attempts to estimate the P-wave velocity in the material applying a frequency estimator that best explains the energy distribution of the possible modes of vibration from the captured IE signals. The velocity estimation will be analysed along a set of freeze-thawing cycles in order to establish a correlation with the internal damage caused in the material confirmed by its porosity. This value has been measured after several freezing-thawing cycles at each stone specimen.

Experimental results show that the proposed method can be considered as a valid and effective tool for determining the internal damage of ornamental stone materials. Besides, the proposed method could be easily adapted to analyse specimens of different sizes, shapes and types of rocks.

1. Introduction

The decay of ornamental stone materials slowly and gradually increases under natural conditions. Nevertheless some porous stones are damaged faster when they are used as building elements. Some weathering mechanisms (e.g. freezing/thawing cycles) cause physical changes and stress within the pore space that lead to granular disintegration and increase porosity. Moreover, in order to gain more knowledge of decay process, accelerated aging tests are frequently carried out with quarry stone probes [42]. However, internal damage is difficult to determine once the stone pieces, which might be cut and carved in different shapes and sizes, are placed in the construction. Therefore, the application of techniques to evaluate the internal quality of ornamental stone materials at an early stage could be very useful.

Non-Destructive Testing (NDT) techniques have been applied in many works in order to assess the quality or properties of stone materials during the last two decades. Specifically, NDT can be defined as the process of inspecting, testing, or evaluating materials in order to search for discontinuities, or differences in certain characteristics without destroying the functionality of the specimen under study [4]. Depending on applications, two approaches based on different types of waves can be employed [7]. The first category is composed of approaches based on electric waves [25,30,38,35,25,2,39,3]. These approaches attempt to determine what defects or imperfections (cavities, fractures and cracks) exist within the block and what is the size, shape or spatial orientation of each defect in order to reduce costs related to the breakage of the stone block. The second category, based on elastic waves, can be split into ultrasonic [6,48,32,43,14] and impact-echo (IE) techniques.

Considering IE approaches, they have been applied by some authors to investigate several materials, such as rock [10,26,44], concrete [17,16,22,24,34,46,47,53,52] or cement [21]. Regarding the proposed signal processing applied to IE signals, the most frequently used technique to evaluate the P-wave velocity is detailed in the guidelines of C138398a [11], which measures the time it takes for the P-wave, generated by an impact, to travel between two transducers that are located at a known distance along the surface of a structure. However, this guideline cannot evaluate small stone materials used as building elements and the accuracy of the P-wave velocity estimates is affected if the distance between the tips of the two transducers is not known accurately. Kassab and Weller [28] performed a study on P-wave velocity in sandstones. For this

* Corresponding author.
E-mail address: vmontiel@ujaen.es (V. Montiel-Zafra).

https://doi.org/10.1016/j.apacoust.2019.05.026
0003-682X/

purpose, the velocity was computed from the porosity of the material, by using a helium porosimeter. Other studies calculated the P-wave velocity from the measured density and the dynamic Young's shear moduli of each test specimen [9]. Besides, some approaches simply applied the Fast Fourier Transform (FFT) to measure the resonant frequency [17,16,22,26,34,44,45]. Although some authors introduced the use of advanced machine learning with IE technique [53], most of them were dedicated to evaluate damage features (defect detection, defect evaluation, defect sizing and location) [17,16,21,22,24,48–51,50,52], to perform a diagnosis of the degradation of the mechanical properties of a material [34] and to compare the resonant frequencies of different materials [10,51]. Finally, some studies analyzed the nonlinear elastic behaviour of damage materials, such as Van Den Abeele et al. [50] and Eiras et al. [21].

This paper proposes a novel method, based on IE, to analyse the internal damage applied to ornamental stone. The contribution of this paper is the estimation of the P-wave velocity applying a frequency analysis that best explains the energy distribution of the possible modes of vibration from the captured IE signals. The velocity estimation will be analysed along a set of freezing-thawing cycles using two heights of impact, three sizes of ball and two stone lithologies, in order to establish a correlation with the internal damage caused in the material confirmed by the porosity testing measured after several freezing-thawing cycles at each stone specimen. The novelty of the proposed method lies in the use of information provided by both frequency and amplitude of the spectral peaks for the estimation of the P-wave velocity, whereas the state-of-the art methods consider only frequency. Besides, the proposed method can be used to assess the global internal structure of the ornamental stone block, i.e., intact or damaged, and it could be easily adapted to analyse specimens of different sizes, shapes and types of rocks.

The remainder of this paper is organized as follows. In Section 2, the types of ornamental stone material are presented in Section 2.1 and the fundamentals of the IE technique are briefly illustrated in Section 2.2. The experimental procedure is described in Section 2.3, the proposed method is detailed in Section 2.4, the reference measurements are explained in Section 2.5 and finally the algorithm for comparison is presented in Section 2.6. Section 3 shows the experimental results. Finally, conclusions and future work are presented in Section 4.

2. Materials and methods

2.1. Samples

Two rock lithologies have been chosen to evaluate the proposed method. The first lithology (hereinafter type 1) corresponds to a biocalcarenite of the local quarry of the village of Porcuna (Jaén, Spain), which is mainly composed of fragments of briozoans and other fossil traces as red algae and parts of echinoderms and pelecipods. The highly fossiliferous stone is scarcely embedded in sparry carbonate cement [40]. This Upper Miocene material has been also used for ornamental purposes. The second lithology (hereinafter type 2) is a biocalcirrudite that is sold under the trade name Amarillo Fossil from Hellín (Albacete, Spain) and it has been usually used as external cladding due to its hydric behaviour and salt resistance, also in historical buildings [33]. This Miocene biocalcirrudite is mainly composed of bioclasts of briozoans, echinoderms and red algae, with grains of quartz as terrigen (5%), bonded by sparite cement.

In this test (see Fig. 1), six ornamental stone blocks have been used for each stone type. Each block is a cube of size $80 \times 80 \times 80\ mm^3$.

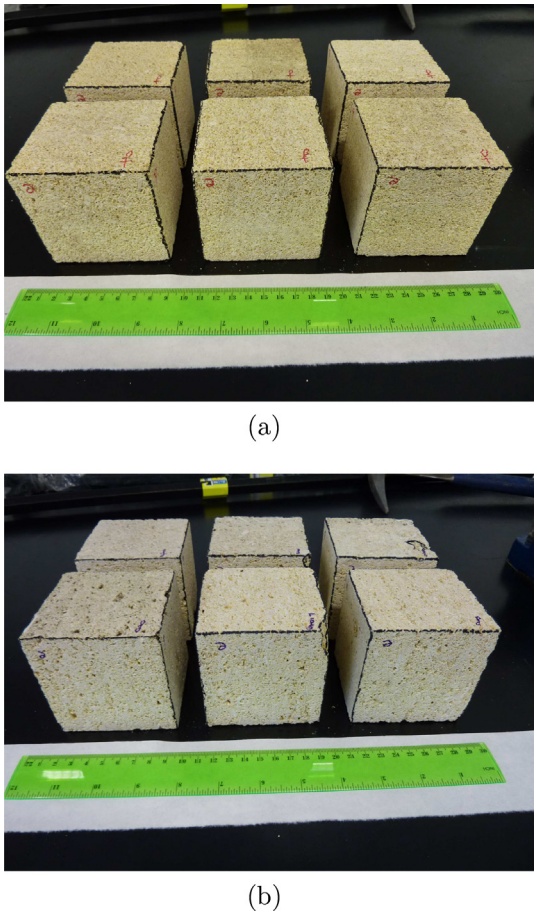

(a)

(b)

Fig. 1. The set of six ornamental stone blocks used in the test: (a) type 1; (b) type 2.

2.2. Impact-echo technique

The impact-echo (IE) method was originally developed by Sansalone and Carino [46] to detect internal flaws in concrete elements. Thereafter, this technique has been applied to investigate the internal quality of other materials [11,26,27]. The acoustic waves are produced by a short duration mechanical impact, usually by using a steel sphere [53] or a hammer at a point on the surface of a solid sample. Three different types of waves are generated by the impact: P-waves (also called longitudinal waves), S-waves (shear or transverse waves) and R-waves (Rayleigh or surfaces waves). P-waves and S-waves propagate into the material along spherical wave fronts, whereas R-waves travel along the surface. It is well known that the internal structure of the material (voids, cracks, interfaces) causes internal reflections of the previous waves [49]. Then, the reflected energy is recorded as a temporal waveform using a sensor or accelerometer mounted adjacent to the impact location. The temporal waveforms are commonly transformed into the frequency domain, because defects are more easily identified in this domain by means of the Fast Fourier Transform (FFT) technique [55,13], which provides a representation that contains most of the waveform energy in significant spectral peaks in the amplitude spectrum.

The input pulse can be approximated as a half sinus curve, with a width (contact time) that is related to the diameter d of the impact ball (in meters). The contact time t_c (in seconds) can be approximated to the following simplified equation [47].

$$t_c = 0.0043d \quad (1)$$

Besides, the amplitude of the frequency components will be proportional to the contact time [12]. The highest frequency f_{max} that can be excited by the impact is a critical parameter. It is dependent on the size of the impact source and should be greater than the frequency of the fundamental mode of vibration of the material. As described in [47], this frequency f_{max} , in kHz, covered by the impact can be estimated using Eq. (2),

$$f_{max} = 291/d \tag{2}$$

The selection of the parameter t_c (in seconds) is a critical issue because the input pulse must contain the correct frequency component [12]. Since the wave propagates back and forth between the top and bottom faces of the evaluated material, the contact time must be chosen according to the total path of the wave (from the impact to the sensor placed at the same face) and the P-wave velocity C_P (in m/s). According to [11], the following condition must be satisfied,

$$t_c < 2T/C_P \tag{3}$$

where T is the thickness (in meters) of the evaluated material. Then, $2T$ represents the propagation path of the wave from the impact to the sensor.

When an impact is applied to a stone material, it is common that not only one frequency is excited, but several vibration modes may appear in the frequency spectrum in which their response is dependent on the shape factor β[51]. This parameter β is dependent on the dimension of the evaluated element [27]. Considering specimens with rectangular cross-sections, β is a depth (D, dimension of the face parallel to the direction of the impact) to breadth (B, dimension of the face perpendicular to the direction of the impact) aspect ratio described by D/B[27]. As previously mentioned in Section 2.1, each block has a dimension $D = 80$ mm and $B = 80$ mm and then a relation of $D/B = 1$, which results on a $\beta = 0.87$[27]. The fundamental mode of vibration (f_1) corresponds to

$$f_1 = \beta\frac{C_P}{2D} \tag{4}$$

Thus, the coefficients required to determine the next five modes of vibration ($f_2 - f_6$), considering $D/B = 1$, are calculated according to [47],

$$f_2 = 1.41f_1, f_3 = 1.9f_1, f_4 = 2.45f_1, f_5 = 2.83f_1, f_6 = 2.34f_1 \tag{5}$$

Finally, the separation between the impact point and the sensor or transducer must be properly chosen. It is commonly acknowledged that this distance should be from 20% to 50% of the maximum depth to be measured [13].

2.3. Experimental procedure

The impact-echo testing instrumentation used in the performance evaluation of the proposed method is described below:

- Mechanical impactors: three steel balls with diameters of 3, 4 and 6 mm.
- Two high-frequency quartz sensor accelerometers (PCB 353B17 [37]). Bandwidth: 0.35 Hz–30 kHz. Sensivity: 10 mV/g.
- Two high-frequency ceramic sensor accelerometers (PCB 352A60). Bandwidth: 5 Hz–60 kHz. Sensivity: 10 mV/g.
- Sensor signal conditioner (PCB 482A18).
- Eight channels audio recorder Zoom F8 with a sampling frequency of 192 kHz per channel.

The impact balls with diameters of 3, 4 and 6 mm get maximum frequencies f_{max} of 97, 72.75 and 48.5 kHz respectively, and the contact times t_c are 0.0129, 0.0172 and 0.0258 ms. The excitation frequency, which is related to material properties and sample dimensions of the specimen, should be lower than both f_{max} and the maximum frequency covered by the accelerometers.

Each impact point is placed at the center of each face of the block. The four sensors mentioned above are located at the diagonals of the same face of the block, at a distance of 1.8 cm from the center of the block, satisfying the condition mentioned in Section 2.2 related to the separation between the impact and the sensor. The three steel balls are dropped from two heights equal to 1 and 1.2 m. By means of the audio recorder, the conditioned signals x(n) are captured and processed using Matlab.

A database has been created to evaluate the proposed method. The database is composed of acoustic signals of one impact. The impact signals have been generated using all possible combinations of balls, heights, sensors and blocks (3 balls × 2 heights × 4 sensors × 6 blocks = 144 signals per type of ornamental rock). Of all the above signals, only 36 impacts signals are subsequently selected considering the signal from the sensor that provides the maximum energy. This selection has been applied due to small variances in the final position of the impact, which slightly varies from the center of the face of the block. Note that the sensor that provides the most reliable impact is used. These ornamental blocks will be subjected to a damage process along freezing-thawing cycles as detailed below. Then, the measurements are conducted before the damage process (hereinafter cycle C0) and then every seven cycles (hereinafter cycles C7, C14, C21 and C28).

2.4. Signal model

The frequency of the fundamental mode of vibration f_1, and so the P-wave velocity is expected to decrease when the damage increases [23,26,36]. For this reason, the proposed method attempts to determine the P-wave velocity using a spectral estimator that takes into account the slight velocity changes according to the real density of the stone block as well as the different modes of vibration active in the spectrum of the IE signal. Specifically, the proposed method adapts the fundamental frequency estimator Non-linear Least-Squares (NLS) [19–19] to include these features.

First, a vector $\mathbf{x}(n)$ composed of N consecutive samples of the observed signal is constructed as follows

$$\mathbf{x}(n) = [x(n)\, x(n+1) \ldots x(n+N-1)]^T \tag{6}$$

where $(\cdot)^T$ denotes the transpose operator and N is the window length. N was empirically estimated, so that the impact signal is completely attenuated.

The covariance matrix is defined as

$$\mathbf{R} = E\{\mathbf{x}(n)\mathbf{x}^H(n)\} \tag{7}$$

where $E\{\cdot\}$ denotes the statistical expectation and $(\cdot)^H$ is the conjugate transpose operator. In practice the covariance matrix is replaced by the sample covariance matrix. First, the autocorrelation is defined as

$$\hat{\mathbf{r}} = \frac{1}{N-M+1}\sum_{m=0}^{N-M}\mathbf{x}(n)\mathbf{x}^H(n-m) \tag{8}$$

with $\hat{\mathbf{r}} = [\hat{r}(-M) \ldots \hat{r}(-1)\, \hat{r}(0)\, \hat{r}(1) \ldots \hat{r}(M)]$ and then the sample covariance matrix $\hat{\mathbf{R}}$ is defined as $\hat{R}(i,j) = \hat{r}(i-j)$.

The pitch estimation problem is defined as follows: a signal $x(n)$ consists of K harmonics with a fundamental frequency ω_0 and corrupted by an additive white Gaussian or colored noise $w(n)$ as

$$x(n) = \sum_{k=1}^{K} a_k e^{jkw_0 n} + w(n) \tag{9}$$

where $a_k = |a_k|e^{j\phi_k}$ with $|a_k| > 0$ and ϕ_k being the amplitude and the phase of the k-th harmonic respectively and the goal is to estimate the fundamental frequency ω_0. As a consequence, the covariance matrix $\mathbf{R}$ can be also written as [17]

$$\mathbf{R} = \mathbf{Z}_0\mathbf{P}\mathbf{Z}_0^H + \sigma^2\mathbf{I} \tag{10}$$

where the diagonal matrix $\mathbf{P}$ contains the squared amplitudes as $\mathbf{P} = diag\left(|a_1|^2 \dots |a_K|^2\right)$, σ^2 is the variance, $\mathbf{I}$ is the identity matrix and the matrix $\mathbf{Z}_0$ has a Vandermore structure being constructed from K harmonics as,

$$\mathbf{Z}_0 = [\mathbf{z}(\omega_0) \dots \mathbf{z}(K\omega_0)] \tag{11}$$

where $\mathbf{z}(\omega) = \left[e^{j\omega} \dots e^{j\omega(N-1)}\right]^T$.

Applying NLS, the fundamental frequency of the signal and amplitudes are estimated by minimizing the 2-norm of the difference between the signal vector and the signal model as,

$$\hat{\omega}_0 = \text{argmin}_{\{\mathbf{a}_k,\omega_0\}}\|\mathbf{x} - \mathbf{Z}_0\mathbf{a}_k\|_2^2 \tag{12}$$

where $\mathbf{a}_k = [a_1 \dots a_K]^T$.

Taking the expected value after replacing $\mathbf{x}$ by the sub-vector $x(n)$, it results in the fundamental frequency estimator that matches it to the covariance matrix [18], which is defined as follows

$$\hat{\omega}_0 = \text{argmax}_{\{\omega_0\}} Tr\left[\mathbf{Z}_0^H\hat{\mathbf{R}}\mathbf{Z}_0\right] \tag{13}$$

where Tr denotes the trace operator.

The NLS-based method is valid for signals composed of a set of harmonics that are multiple of ω_0. However, the IE signal is non-harmonic and it consists of a set of modes of vibration. As an example, Fig. 2 shows the FFT applied to $\hat{\mathbf{R}}$ of an IE signal belonging to an ornamental stone block of type 1 at cycle C0. For the database, $N = 801$ samples, $M = 400$ samples and a 12816-points FFT is computed.

Subsequently, we propose a modified NLS algorithm for estimating modes of vibration. Then, a frequency estimation problem is defined: an IE signal consists of L modes of vibration, which can be written as

$$x(n) = \sum_{l=1}^{L} a_l e^{j\omega_l n} + w(n) \tag{14}$$

where $\omega_l = [\omega_1\ \omega_2 \dots \omega_L]$ and $a_l = [a_1\ a_2 \dots a_L]$ are the frequencies and the amplitudes of the L modes of vibration related to Eqs. (4) and (5) respectively. According to [19], the NLS estimator is efficient (low signal-to-noise ratio) for white or colored noise.

The frequency of the fundamental mode of vibration ω_1 is estimated as follows,

$$\hat{\omega}_1 = \text{argmin}_{\{\mathbf{a}_l,\omega_1\}}\|\mathbf{x} - \mathbf{Z}_1\mathbf{a}_l\|_2^2 \tag{15}$$

where $\mathbf{a}_l = [a_1 \dots a_L]^T$ and $\mathbf{Z}_1$ is constructed from the L modes of vibration as

$$\mathbf{Z}_1 = [\mathbf{z}(\omega_1) \dots \mathbf{z}(\omega_L)] \tag{16}$$

Besides, as indicated in Eq. (13), the fundamental mode of vibration ω_1 that best explains the energy distribution considering the spectral locations of the associated modes of vibration active in the spectrum of the IE signal can be estimated using the expected value as shown in Eq. (17),

$$\hat{\omega}_1 = \text{argmax}_{\{\omega_1\}} Tr\left[\mathbf{Z}_1^H\hat{\mathbf{R}}\mathbf{Z}_1\right] \tag{17}$$

To illustrate the performance of the proposed method, the example shown in Fig. 2 is analysed. Assuming a P-wave velocity range from 1850 to 2400 m/s, the spectral range of the fundamental frequency f_1, associated to the fundamental mode of vibration, which corresponds to the previous velocity range varies from 10.06 kHz to 13.05 kHz. This is going to be the used range of values for ω_1 at the estimator of Eq. (17). Fig. 3 shows the range of frequency in which the estimator searches for the fundamental mode of vibration. It can be observed that the proposed method estimates the next modes of vibration:$f_1 = 11.73$ kHz (in red color), $f_2 = 16.54$ kHz, $f_3 = 22.29$ kHz, $f_4 = 28.74$ kHz, $f_5 = 33.19$ kHz, $f_6 = 27.45$ kHz. The selection of the fundamental mode of vibration f_1 does not exactly match to the peak on Fig. 3 since the presence of the next five modes of vibration influences the selection of ω_1 as indicated in Eq. (17). Anyway, three of the frequency peaks (first, second and sixth) coincide with the highest peaks of the spectrum. This result is a consequence of the selection of the main mode of vibration, which depends on the other five modes as shown in Eq. (17) and the second and the sixth modes are the highest peaks apart from the main mode. Indeed, the dashed black line in Fig. 3 shows the expected value of the estimator when evaluating the trace $Tr\left[\mathbf{Z}_1^H\hat{\mathbf{R}}\mathbf{Z}_1\right]$ of Eq. (17) along the P-wave velocity range. When

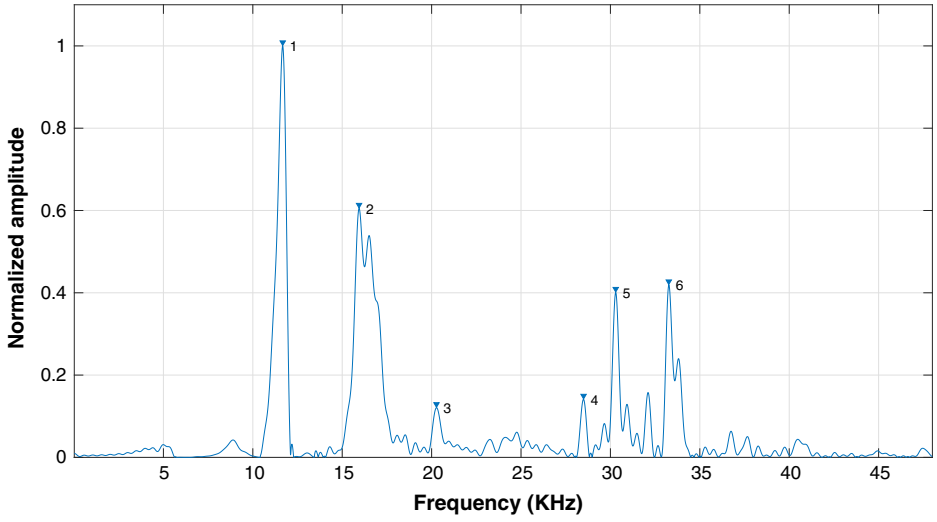

Fig. 2. FFT of $\hat{\mathbf{R}}$ of a signal measured by a ceramic sensor placed at the block number 1 of type 1 when using a ball with a diameter of 4 mm and an impact height of 1.2 m before the damage process (C0). The inverted triangles mark the six highest isolated peaks.

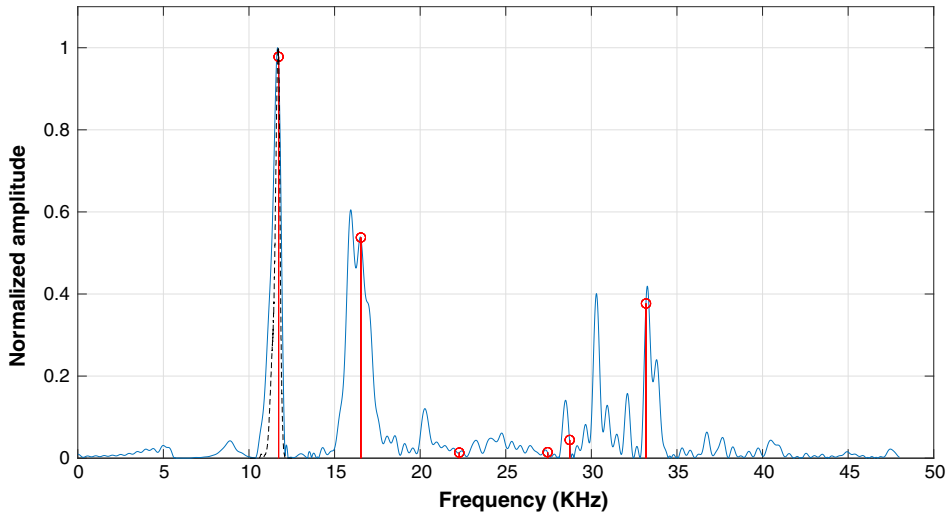

Fig. 3. FFT of $\hat{\mathbf{R}}$ shown in Fig. 2. It can be seen that the proposed method searches for the fundamental mode of vibration inside the defined spectral range, providing a frequency estimation (in red colour) $f_1 = 11.73$ kHz.

computing the trace, the six modes of vibration are used for defining $\mathbf{Z}_1$ of Eq. (16). The estimated fundamental mode of vibration $\hat{\omega}_1$ is selected as the maximum value, as defined in Eq. (17). In this way, the combination of six modes of vibration that maximizes the trace and, therefore, best defines the spectrum of the signal is finally estimated as the frequency of the fundamental mode of vibration. From this value, we obtain the estimation of the P-wave velocity. Finally, the estimated fundamental mode of vibration results in a C_P of 2157 m/s.

Considering the same combination of height-ball-block and the four sensors used, only the signal from the sensor that provides the highest energy in the captured signal is selected for further analysis. The normalized energy E_n is calculated taking into account the energy present in the frequencies related to the fundamental and the next five modes of vibration for a range of C_P from 1850 to 2400 m/s and normalizing it with respect to the total energy of the spectrum. Besides, assuming that P-wave velocity cannot be correctly estimated when the energy is low, $E_n < 0.6$, we have only chosen P-wave values obtained using a normalized energy higher than this threshold $th = 0.6$ that has been empirically determined from preliminar analysis.

Summarizing, the proposed method is implemented through the following steps:

1. Capturing the IE signals belonging to the four sensors.
2. Selecting the signal with maximum energy from the four sensors.
3. Windowing N samples of the signal.
4. Estimating $\hat{\mathbf{R}}$ with $M = N/2$.
5. Applying Eq. (17) for C_P values between 1850 and 2400 m/s with resolution of 1 m/s.
6. Computing the normalized energy E_n estimated by the proposed method as the relation between the energy present in the frequencies related to the fundamental and the next five modes of vibration and normalizing it with respect to the total energy of the spectrum.
7. Estimating the C_P when $E_n > 0.6$.

2.5. Reference measurements

To calculate the reference P-wave velocities used by the proposed algorithm in order to create a database and evaluate its performance, several reference measurements must be performed.

The velocity of the acoustic waves generated by the impact depends on the structural and material properties of the specimen. Correlating the changes in these properties with the measured velocity helps to evaluate the degree of stone deterioration [8]. Porosity is one of the most important physical features controlling this deterioration [1,41]. Then, it is expected that stones with higher porosity will suffer a higher level of deterioration compared with stones with lower porosity.

Freezing-thawing cycles aging tests were performed in order to generate stresses within each stone block increasing the porosity and generating cracks. For each block, the procedure consisted in twenty-eight cycles (C1–C28) of 24-h where each of them was water-saturated and then exposed to freezing temperatures [41]. Each block is cyclically loaded by cooling in a freezer with a temperature of – 15 °C for 18 h and thawing in water for 6 h (room temperature 20–22 °C).

To acquire additional information about the block deterioration, the measurement of the Connected Capillary Porosity (CCP) was carried out before the damage process C0 and then after every seven cycles (C7, C14, C21 and finally C28). The value of $CCP(\%)$, which corresponds to inter-connected pores with radius > 0.1 μm, was estimated as the ratio of the mass of water by capillary uptake M_s to cubic sample volume V_c and water density $\rho_a \left(CCP(\%) = \left(\frac{M_s}{V_c - + \rho_a} \right) * 100 \right)$ [20].

Hereafter, a velocity analysis must be performed to establish a correlation between the internal damage of each stone block when each IE signal is processed. The P-wave velocity C_P is measured along the freezing-thawing cycles. Using the IE method, it is common to measure the P-wave velocity following the guidelines of procedure A of C138398a [11]. An impact is applied on a block to generate transient stress waves, which propagate along its surface. Two sensors are placed on a line at a known distance l apart. Then, it is possible to determine the P-wave velocity by dividing the time difference by this distance l. This procedure requires a distance l of 300 mm between sensors, whereas the distance between the impactor and the first sensor should be of 150 ± 10 mm, so this guideline cannot evaluate stone materials used as building elements with a size smaller than 450 mm. Then, a dry block with a size of $500 \times 100 \times 2$ mm^3 of both types of ornamental stone has been used in order to measure the P-wave velocity in each material. The position of the impactor has been located at a distance of 150 mm from the first sensor. The distance between the two sensors is $l = 300$ mm and the time difference (the travel time) is

calculated as the time elapsed until the voltage of the captured signal by the sensors changes from the the base line value. Twelve impacts have been performed in different places of the block and the estimated P-wave velocity has been calculated as the mean of these velocity values. Specifically, a $C_{P_1} = 2057$ m/s has been estimated for type 1 blocks and $C_{P_2} = 2272$ m/s for type 2 blocks. Note that our empirical measures, evaluating both types of ornamental stone, are consistent with those ones obtained in [31] in which the P-wave velocity varies from 2000 to 3000 m/s.

2.6. Algorithm for comparison

In order to evaluate the performance of the proposed method, an algorithm for comparison has been implemented. In [5], Bernard et al. proposed a Bayesian formulation of the resonant ultrasound spectroscopy inverse problem to recover the viscoelastic properties of anisotropic attenuative solid materials. The method of [5] requires the estimation of the resonant frequencies. This step is implemented using a state-of-the-art method based on a linear prediction filter (initially proposed by Kumaresan and Tufts [29]) refined by a non-linear fitting to improve the repeatability of the parameter estimation. In this work, we have used the same approach, the method proposed by Kumaresan and Tufts [29] and the non-linear fitting introduced by Bernard et al. [5], for comparison purposes. Finally, the fundamental frequency is calculated by minimizing a cost function used by Bernard et al. of the type

$$F = \sum_{n=1}^{6} \left(\frac{f_n^{exp} - f_n^{model}}{f_n^{exp}} \right)^2 \tag{18}$$

which paires the measured frequency (f_n^{exp}) and the corresponding predicted frequency (f_n^{model}) of Eq. (5) for C_P values between 1850 and 2400 m/s with resolution of 1 m/s.

3. Experimental results

The values of $CCP(\%)$ for the undamaged blocks and after every seven cycles are shown in Table 1. It can be observed that CCP values of blocks 1–6 of each stone type are very similar before the damage process (C0). It can be seen that all blocks of type 1 show higher CCP than blocks of type 2. Moreover, blocks of type 1 present a total rise of the CCP value of 5% in comparison with an increase of 2–3% for blocks of type 2. The difference of the CCP values between blocks of type 1 and type 2 can be related to the specific lithology of each material as mentioned in Section 2.1. Finally, these results suggest that between cycles C21 and C28 the CCP values do not change significantly.

Consequently, a visual analysis of the blocks state is performed. Once the twenty-eight cycles (C28) are completed, the state of each block, labelled as type 1, is detailed below:

- Block 1: no cracks
- Block 2: important crack in two faces
- Block 3: important crack in one face
- Block 4: important crack in three faces
- Block 5: small fractures
- Block 6: no cracks

The most damaged blocks (2, 3 and 4) can be observed in Fig. 4. On the other hand, type 2 blocks appearance remains unchanged. These results are consistent with the CCP values present in Table 1. The presence of fissures or small cracks in the surface do not imply a significant increase of the total CCP value, already very high in cycle C28. The description of both lithologies, previously explained in Section 2.1, and this visual inspection indicate that the stone material of type 2 seems to be stiffer than type 1. The measurements of the IE signals $x(n)$ were carried out during the C0, C7, C14, C21 and C28 cycles. The measured signals will be compared to the CCP values in order to establish a correlation between the damage, porosity and IE response of the ornamental stone evaluated.

Fig. 5 shows P-wave velocity analysing blocks belonging to type 1 and type 2. Each box represents thirty-six data points, one for the seven cycles evaluated (C0, C7, C14, C21 and C28) using the mentioned threshold *th*. The lower and upper lines of each box show 25th and 75th percentiles of the P-wave velocity estimates. The line in the middle of each box corresponds to the median. The lines extending above and below each box show the extent of the rest of the P-wave velocity estimates. Finally, outliers are plotted as individual red points. Considering blocks type 1, Fig. 5(a) reports that the median of the P-wave velocity is about 2122 m/s analysing cycle C0, a value similar to that estimated in Section 2.5. In cycle C7 the median value of P-wave velocity, 2114 m/s, has decreased compared to cycle C0. In cycle C14 the median value is 2038 m/s, whereas in cycle C21 the median value has significantly decreased to 1903 m/s. The decreasing trend is evident: the median P-wave velocity has exponentially been reduced from cycles C0 to C21. However, when the blocks are completely damaged as occurs in C28, the median velocity is stabilized (C_P = 1911 m/s) showing a high increase of the velocity dispersion. As the dispersion increases, the reliability of the data is reduced and as a consequence, the quality of the material is questionable. Besides, C_P is directly related to the dimension of the block (Eq. (4)). The presence of fractures in the blocks in cycle C28 results in an alteration of the aspect ratio and then the estimation of the frequency f_1 could change severely. To summarize, there is a reduction of approximately 8 m/s between C0–C7, 76 m/s comparing C7–C14,

Table 1
$CCP(\%)$ of each block after C0, C7, C14, C21 and C28 freezing-thawing cycles.

Type	Block	C0	C7	C14	C21	C28
1	1	21,92%	22,78%	23,67%	26,14%	26,40%
1	2	19,69%	20,65%	21,66%	23,97%	24,46%
1	3	16,44%	18,20%	20,14%	23,04%	22,86%
1	4	19,69%	20,59%	21,52%	24,51%	24,45%
1	5	18,61%	19,61%	20,66%	23,32%	23,05%
1	6	19,73%	20,65%	21,61%	24,07%	23,42%
2	1	15,32%	15,89%	16,48%	18,27%	18,10%
2	2	15,63%	16,04%	16,46%	18,01%	17,99%
2	3	15,43%	15,74%	16,06%	17,57%	17,68%
2	4	15,93%	17,30%	18,79%	18,27%	18,06%
2	5	15,34%	14,84%	14,36%	18,03%	18,02%
2	6	15,43%	15,95%	16,49%	17,97%	18,01%

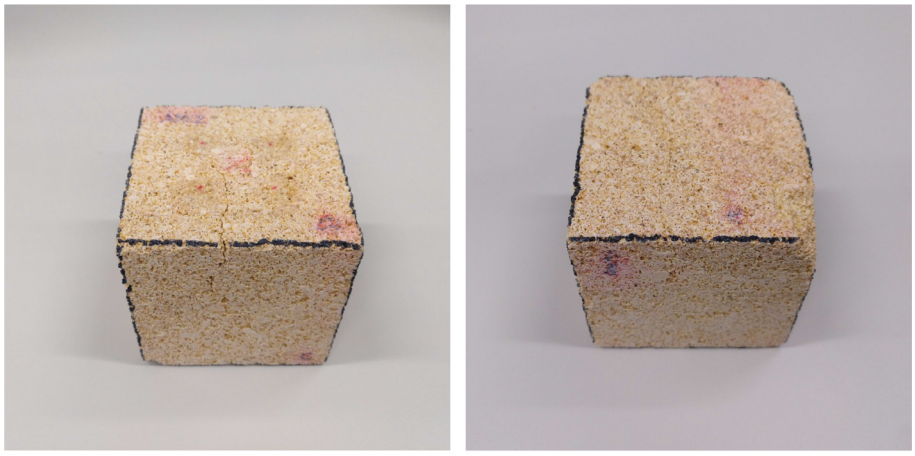

(a) Block 2 (b) Block 3

(c) Block 4

Fig. 4. Some of the blocks of type 1 that have suffered breakage: (a) Block 2 shows a crack in two of its faces; (b) Block 3 exhibits only one crack in one of its faces; (c) Block 4 presents a big fracture in three of its faces.

135 m/s comparing C14–C21, an increase of 8 m/s comparing C21–C28 and finally a total of 211 m/s between C0–C28. The decrease of the P-wave velocity is not constant: when the block is not damaged, the velocity suffer a small decrease. However, this decrease is higher as the damage of the block is starting to occur as shown in cycles C14 and C21. Finally, when the block is completely damaged, the decrease of the velocity comparing two consecutive cycles C21–C28 is lower as can be observed in Fig. 5(a). Moreover, it is clear that when the blocks are intact, in the case of C0 or quasi-intact in C7 and C14, the dispersion is lower compared to damaged blocks in the cycles C21 and C28.

Fig. 5(b) shows that the median velocity for cycle C0 is located at 2256 m/s, which is correlated to the measured value of Section 2.5. For cycle C7, the P-wave velocity has decreased to 2227 m/s. In the case of cycle C14, a median velocity of 2217 m/s is estimated. Then, cycle C21 presents a median velocity of 2200 m/s and many outliers appear at lower velocities. Finally, for cycle C28 the velocity is diminished to 2184 m/s. This decreasing trend is clearly related to the CCP values shown in Table 1 and it is not as pronounced as the type 1 slope. There is low variability in the P-wave velocity comparing consecutive cycles. This trend suggests that the blocks of type 2 are not damaged as confirmed by the CCP values in Section 2.5 and the visual inspection of the blocks, which have no visible damage and appear to be intact. This fact is shown in Fig. 5 when comparing the box of C28 of type 2 and the box of C0 of type 1, which are really similar. Then, the P-wave velocity of the blocks of type 2 along the cycles suffer lower decrease than the velocity related to type 1. In fact, there is a total reduction of only 72 m/s, compared with the reduction of 211 m/s of the blocks of type 1. It can be explained, once again, because the lithology of type 2 is more compact and robust, then the porosity is lower and the damage is minor respect to type 1. In general terms, the dispersion of the data for each cycle does not vary significantly. This technique can be an indicator about the internal quality of a material, i.e. using information about the level of porosity of the internal structure of the ornamental stone.

Fig. 5(c) and (d) show P-wave velocity analysing blocks belonging to type 1 and type 2 by applying the state-of-the-art algorithm described on Section 2.6. Considering blocks type 1, it can be observed a clear decreasing trend as occurs in Fig. 5(a). However, the median velocity of the P-wave velocity estimation found by the algorithm [5] for cycle C28 is much smaller than for the proposed method. Considering Fig. 5(d), the median velocity of the P-wave velocity estimation found by the algorithm for comparison is not correlated with the number of cycles, as can be seen the median velocity decreases for cycles C21 and C28 from the value

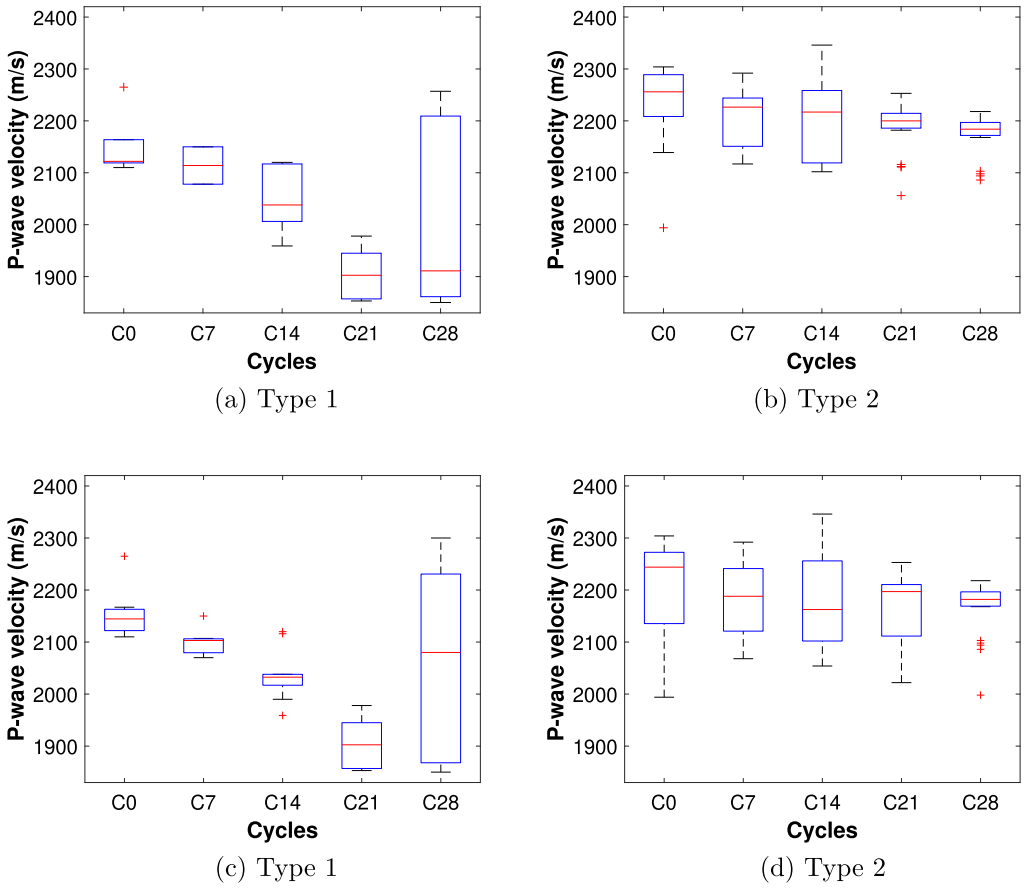

Fig. 5. P-wave velocity vs freezing-thawing cycles for stone blocks after applying a threshold $th = 0.6$ of the normalized energy estimated by the proposed method: (a) type 1 and (b) type 2, and by the algorithm described on Section 2.6: (c) type 1 and (d) type 2.

of C14. for comparison presents an evident fluctuation: from cycle C14 to C21 the velocity increases and the velocity in cycle C28 is higher than in cycle C14, whereas the proposed method shows a decreasing velocity.

Finally, Fig. 6 shows the median C_P estimated by the proposed method compared with the median CCP value of Table 1 after every seven freezing-thawing cycles. Then, five pairs of C_P-CCP points for cycles C0, C7, C14, C21 and C28 are plotted. Although it can be appreciated a linear relation between both parameters for each type of evaluated stone, each type of stone reports a different slope of the linear regression because each slope is more pronounced as the damage of the material increases, as expected. Therefore, the proposed method has demonstrated to be a suitable tool to determine the internal damage of a material without carrying out measures of the CCP value. The measurement of the C_P of the material would require a reference stone block cut and safe from adverse

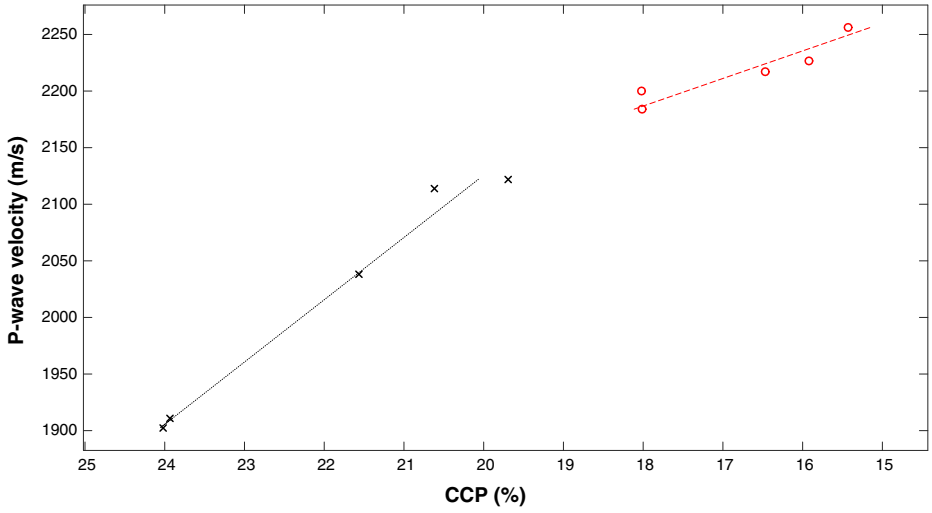

Fig. 6. Median P-wave velocity estimated vs median *CCP*(%) after every seven freezing-thawing cycles: blocks type 1 (in black crosses) and type 2 (in red circles). The best fitted linear regression models are shown by the dashed lines.

weather conditions. However, in the case of building elements that have been placed in the construction the CCP measurement would not be feasible and the proposed method would offer a competitive advantage. Besides, the performance of the proposed method is independent of the diameter of the impactors while the frequencies related to the modes of vibration were lower than the f_{max} excited by the balls of the impactors.

4. Conclusions

The IE method, one of the many NDT techniques, has been widely used for detecting internal defects of different materials. Besides, the interpretation of the results usually involves a simple spectrum analysis, which does not take into account the frequencies related to the different modes of vibration. The main contribution of this paper is the estimation of the P-wave velocity applying a frequency analysis that best explains the energy distribution of simultaneous modes of vibration active in the spectrum of the acoustic signal.

A database has been created to evaluate the proposed method. The database is composed of acoustic signals of one impact. The impact signals have been generated using all possible combinations of balls, heights and blocks and selecting those that come from the sensor that captures the most energy of each combination. These ornamental blocks have been subjected to a damage process along freezing-thawing cycles in order to establish a correlation between the damage and the P-wave velocity estimation provided by the proposed method.

The proposed technique has been evaluated in experimental testing and it has given promising results, indicating that it is a suitable tool to provide reliable and useful information about the internal damage of the structure of the ornamental stone material. The capabilities of an IE system to help with evaluating the global internal quality of stone materials has been demonstrated. Highlight as advantage that the proposed method can be easily adapted to analyse different ornamental stone specimens of different lithology and sizes. Results demonstrate that, on the whole, the P-wave velocity (or the frequency related to the fundamental mode of vibration) decreases when the damage of the stone increases due to a higher percentage of porosity. Besides, the proposed method can be considered a valid tool to investigate the porosity of a stone material, offering information of quality control. On the other hand, it has been demonstrated that it is not possible to determine the type, shape or spatial orientation of the possible defects in stone products. The application of this method requires a reference stone block that had been cut and healthy from adverse weather conditions. The range of frequencies of the proposed method should be adapted to the dimensions of the specimen to be analysed. Moreover, the analysis of the recorded IE signals indicates that it is a crucial issue to correctly define the energy of the impacts. Finally, future work will focus on evaluating the phase differences of the IE signals of the four sensors for each block in order to get useful information about the propagation of the P-wave. Moreover, an interesting research direction will be to analyse the combination of the measured P-wave and S-wave velocities with respect to the porosity of the material as well as on evaluating the non-linear behaviour by modifying the type of the impact.

Declaration of Competing Interest

V. Montiel has received a research grant from the Andalusian Business, Science and Innovation Council under Project P11-TIC-7278. F. Canadas-Quesada, M. J. Campos-Suñol, P. Vera-Candeas and N. Ruiz-Reyes declare that they have no conflict of interest.

Acknowledgments

This work was performed using funds provided by the Andalusian Business, Science and Innovation Council under Project P11-TIC-7278. The authors would like to thank the anonymous reviewers for their well informed and helpful suggestions that greatly contributed to improve the final version of the manuscript.

References

[1] Akin M. Evaluation of the long-term durability of yellow travertine using accelerated weathering tests; 2011: 101–114.
[2] Arosio D, Munda S, Zanzi L. Quality control of stone blocks during quarrying activities. In: 14th International Conference on Ground Penetrating Radar (GPR), Shangai, China.
[3] Arosio D. Rock fracture characterization with GPR by means of deterministic deconvolution. J Appl Geophys 2016;126:27–34.
[4] The American Society for Nondestructive Testing; 2018. URL: https://www.asnt.org/MinorSiteSections/AboutASNT/Intro-to-NDT [accessed 20.06.2018].
[5] Bernard S, Grimal Q, Laugier P. Resonant ultrasound spectroscopy for viscoelastic characterization of anisotropic attenuative solid materials. J Acoust Soc Am 2014;135(5):2601–13.
[6] Bramanti M, Bozzi E. A procedure to detect flaws inside large sized marble rocks by ultrasound. SSTA Appl 2001;2:1–13.
[7] Bodare A. Non destructive test methods of cultural stone. In: Published Report 3017, Division of Soil and Rock Mechanics. Stockholm: Department of Civil and Environmental Engineering, Royal Institute of Technology; 1996.
[8] El Boudani M, Wilkie-chancellier N, Martinez L, Hebert R. Marble characterization by ultrasonic methods. Procedia Earth Planet Sci 2015;15:249–56.
[9] Brant LC, Nikolaou S, Moss C. Resonant frequency testing of New York City rock types. Geotech Test J 2013;36(4):466–75.
[10] Bunget G, Shen Q, Gramling F, Judd D, Kurfess TR. Impact-acoustic evaluation method for rubber – steel composites: Part I. Relevant diagnostic concepts. Appl Acoust 2015;90:74–80.
[11] C1383-98a. Standard test method for measuring the P-wave speed and the thickness of concrete plates using the impact-echo method. Am Soc Test Mater 1998.
[12] Carino NJ. The impact-echo method: an overview. Structures, 1–18. Reston, VA: American Society of Civil Engineers; 2001.
[13] Carino NJ. Impact echo: the fundamentals principles of impact-echo method. Int Symp Non-Destruct Test Civil Eng 2015.
[14] Cerrillo C, Jimenez A, Rufo M, Paniagua J, Pachon F. New contributions to granite characterization by ultrasonic testing. Ultrasonics 2014;54:156–67.
[15] Colla C, Lausch R. Influence of source frequency on impact-echo data quality for testing concrete structures. NDTE Int 2003;36(4):203–13.
[16] Chaudhary MTA. Effectiveness of Impact Echo testing in detecting flaws in prestressed concrete slabs. Constr Build Mater 2013;47:753–9.
[17] Christensen MG, Jakobsson A. Improved subspace-based frequency estimation for real-valued data using angles between subspaces. Eur Signal Process Conf 2010;4:358–62.
[18] Christensen MG, Jakobsson A. Multi-pitch estimation. Synthesis lectures on speech and audio processing. Morgan & Claypool Publishers; 2009. ISBN:9781598298383.
[19] Christensen MG, Stoica P, Jakobsson A, Holdt Jensen S. Multi-pitch estimation. Signal Process 2008;88(4):972–83.
[20] Cueto N, D del-Cura MA. Influence of anisotropy on rock hydrical properties. Analysis of brecciated dolostones from Betic Cordillera (Spain). Geogaceta 2006;40:315–8. ISSN 0213-683X.
[21] Eiras J, Monzo J, Payá J. Non-classical nonlinear feature extraction from standard resonance vibration data for damage detection. J Acoust Soc Am 2014;135(2). EL82.
[22] Garbacz A, Piotrowski T, Courard L, Kwasniewski L. On the evaluation of interface quality in concrete repair system by means of impact-echo signal analysis. Constr Build Mater 2017;134:311–23.
[23] Grandjean G, Gourry JC. GPR data processing for 3D fracture mapping in a marble quarry (Thassos, Greece). J Appl Geophys 1996;36:19–30.
[24] Hsiao C, Cheng C, Liou T, Juang Y. Detecting flaws in concrete blocks using the impact-echo method. NDTE Int 2008;41(2):98–107.
[25] Hugenschmidt J, Kalogeropoulos A, Soldovieri F, Prisco G. Processing strategies for high-resolution GPR concrete inspections. NDTE Int 2010;43:334–42.
[26] Johnson PA, Zinszner B, Rasolofosaon PNJ. Resonance and elastic nonlinear phenomena in rock. J Geophys Res Solid Earth 1996.
[27] Jording AC. Damage detection in metamorphic stone blocks utilizing impact-echo testing and modal analysis [Ph.D. thesis]; 2012.
[28] Kassab MA, Weller A. Study on P-wave and S-wave velocity in dry and wet sandstones of Tushka region, Egypt. Egypt J Petrol 2015;24(1):1–11.
[29] Kumaresan R, Tufts D. Estimating the parameters of exponentially damped sinusoids and pole-zero modeling in noise. IEEE Trans Acoust Speech Signal Process 1982;30(6):833–40.
[30] Lualdi M, Zanzi L. 2D and 3D GPR imaging to map the fractures and to evaluate the integrity of limestone ornamental rocks. In: Proceedings of the Symposium

on the Application of Geophysics to Environmental and Engineering Problems (SAGEEP03), San Antonio, Texas, USA. p. 613–22.
[31] Mavko G. Conceptual overview of rock and fluid factors that impact seismic velocity and impedance. Stanford Rock Physics Laboratory; 2005. p. 112.
[32] Onur AH, Bakrac S. Determination of discontinuities in marble blocks via a nondestructive ultrasonic technique. Int J Min Met Mater 2009;16:487–93.
[33] Ordonez S, García del Cura MA, Bernabeu A, Rodríguez MA. Rocas ornamentales porosas del Mioceno marino de Levante (Alicante-Murcia-Albacete). Avances en el conocimiento del Terciario Ibrico. Madrid: UCM; 1997. p. 141–4.
[34] Park SJ, Yim HJ. Evaluation of residual mechanical properties of concrete after exposure to high temperatures using impact resonance method. Constr Build Mater 2016;129:89–97.
[35] Pasolli E, Melgani F, Donelli M. Automatic analysis of GPR images: a pattern-recognition approach. IEEE Trans Geosci Remote 2009;47(7).
[36] Payan C, Garnier V, Moysan J, Johnson PA. Applying nonlinear resonant ultrasound spectroscopy to improving thermal damage assessment in concrete. J Acoust Soc Am 2007;121(4):EL125–30.
[37] PCB Piezotronics; 2018. URL: http://www.pcb.com/Home [accessed 1.10.2018].
[38] Porsani JL, Sauck WA, Junior AOS. GPR for mapping fractures and as a guide for the extraction of ornamental granite from a quarry: a case study from southern Brazil. J Appl Geophys 2006;58:177–87.
[39] Rey J, Martinez J, Vera P, Ruiz N, Canadas F, Montiel V. Ground-penetrating radar method used for the characterisation of ornamental stone quarries. Constr Build Mater 2015;77:439–47.
[40] Roldán FJ. Estudio Geológico de las Unidades Neógenas comprendidas entre Espejo y Porcuna (provincias de Córdoba y Jaén)', Depresión del Guadalquivir [Ph.D. Thesis]. Universidad de Granada; 1988.
[41] Ruedrich J, Kirchner D, Siegesmund S. Physical weathering of building stones induced by freeze-thaw action: a laboratory long-term study. Environ Earth Sci 2011;63(7):1573–86.
[42] Ruedrich J, Siegesmund S. Salt and ice crystallisation in porous sandstones. Environ Geol 2007;52(2):343–67.
[43] Saez-Perez MP, Rodriguez-Gordillo J. Structural and compositional anisotropy in Macael marble (Spain) by ultrasonic, XRD and optical microscopy methods. Constr Build Mater 2009;23:2121–6.
[44] Sadri A. Application of impact-echo technique in diagnoses and repair of stone masonry structures. NDTE Int 2003;36(4):195–202.
[45] Salazar A, Vergara L, Gosalbez J. Blind source separation for classification and detection of flaws in impact-echo testing. Mech Syst Signal Pr 2005;19 (6):1312–25.
[46] Sansalone M, Carino NJ. Impact echo: a method for flaw detection in concrete using transient stress waves NBSIR 86-3452. National Bureau of Standards; 1986.
[47] Sansalone M, Streett W. Nondestructive evaluation of concrete and masonry. Ithaca, NY: Bullbrier Press; 1997.
[48] Sarpun IH, Kilickaya MS. Mean grain size determination in marbles by ultrasonic backwall echo height measurements. NDTE Int 2006;39:82–6.
[49] Steber GR, Ghorbanpoo A. Detection and processing of impact echoes in concrete. In: Industrial Electronics Society. IECON90, 16th Annual Conference of IEEE. p. 340–5.
[50] Van Den Abeele K, Sutin A, Carmeliet J, Johnson P. Micro-damage diagnostics using nonlinear elastic wave spectroscopy (NEWS). NDTE Int 2001;34 (4):239–48.
[51] Wang JJ, Chang TP, Chen BT, Lin HC, Wang H. Evaluation of resonant frequencies of solid circular rods with impact-echo method. J Nondestruct Eval 2010;29(2):111–21.
[52] Xie Z, Zhang Y, Wu H. Automated data fusion and visualization for impact-echo testing of concrete structures. IEEE Sens J 2012;12(12):3346–53.
[53] Zhang JK, Yan W, Cui DM. Concrete condition assessment using impact-echo method and extreme learning machines. Sensors (Switzerland) 2016;16 (4):1–17.